



Enhanced fluorescence/magnetic resonance dual imaging and gene therapy of liver cancer using cationized amylose nanoprobe



Hanchen Zhang^{a,b,c,1}, Li Deng^{d,1}, Haiqing Liu^{a,b,1}, Siyao Mai^{a,b}, Ziliang Cheng^{a,b}, Guangzi Shi^{a,b}, Hong Zeng^{e,b}, Zhuo Wu^{a,b,*}

^a Department of Radiology, Sun Yat-Sen Memorial Hospital, Sun Yat-Sen University, Guangzhou, 510120, China

^b Guangdong Provincial Key Laboratory of Malignant Tumor Epigenetics and Gene Regulation, Medical Research Center, Sun Yat-Sen Memorial Hospital, Sun Yat-Sen University, Guangzhou, 510120, China

^c Department of Nuclear Medicine, The Sixth Affiliated Hospital, Sun Yat-sen University, Guangzhou, 510655, China

^d Institute of Nano and Biopolymeric Materials, School of Materials Science and Engineering, Tongji University, 4800 Caoan Road, Shanghai, 201804, China

^e Department of Pathology, Sun Yat-Sen Memorial Hospital, Sun Yat-Sen University, Guangzhou, 510120, China

ARTICLE INFO

Keywords:

Amylose

Nanoparticles

Hepatocellular carcinoma

Magnetic resonance imaging

Fluorescence imaging

Gene therapy

ABSTRACT

Recently, various technologies for targeted gene release in cancer treatment have emerged. However, most of these strategies are facing the challenge of untraceable distribution and poor antitumour treatment effects. In this study, we constructed a gene delivery system that integrated a series of components to assemble multifunctional NPs, providing a promising therapeutic nanopatform for hepatocellular carcinoma (HCC) therapy. Cationized amylose (CA), superparamagnetic iron oxide (SPIO) nanoparticles (NPs), and tetraphenylethylene (TPE) were self-assembled to form nanospheres (CSP/TPE). The prepared NPs was modified with SP94 peptide through amidation reaction, and then survivin small interfering RNA (siRNA) were loaded into the NPs to form CSP/TPE@siRNA-SP94 NPs. Our results showed that the prepared NPs had good size distribution, high RNA condensation and transfection ability. CSP/TPE@siRNA-SP94 NPs exhibited excellent fluorescence and magnetic resonance (MR) imaging properties *in vitro* and *in vivo*. The prepared targeted NPs improved Huh-7 cellular uptake *in vitro*, and the biodistribution of CSP/TPE@siRNA-SP94 *in vivo* was observed through *in/ex vivo* fluorescence imaging system and MRI. As survivin siRNA effectively retained in tumour cells, CSP/TPE@siRNA-SP94 NPs considerably inhibited tumour growth *in vivo*. In addition, H&E staining results showed that all the prepared CSP-based NPs had good biocompatibilities, as few histological changes or tumour metastasis were observed in major organs of the mice in the treatment group. Therefore, we envisage that the prepared CSP/TPE@siRNA-SP94 NPs can represent a promising strategy for HCC diagnosis and treatment.

1. Introduction

In 2020, hepatocellular carcinoma (HCC) ranks the fourth among the leading cause of cancer-related death worldwide [1]. In clinical practice, there are a few patients diagnosed early; while patients with advanced HCC are only suitable for ablative therapy, chemoembolization and systemic therapy [2]. As gene therapy shows great prospects in the treatment of human diseases through the precise regulation of gene expression [3,4], it has been recognized as one of the future development directions of HCC treatment [5,6]. The pathogenesis of multi-stage liver cancerization gradually evolves through the inflammatory responses that trigger genetic changes. This would lead to the imbalance of multiple

signalling pathways and the formation of heterogeneous parenchymal tumours. Survivin protein overexpressed in HCC cells can significantly inhibit cell apoptosis and promote tumour tissue proliferation [7]. Survivin small interfering RNA (siRNA) has been used to suppress the protein expression by silencing survivin mRNA, hence triggering the apoptosis of HCC cells [8]. Although *in vitro* experiments have shown that survivin siRNA gene has high efficacy in the suppression of HCC growth [9], there are still some obstacles in delivering siRNA to specific cells. For example, siRNA can be degraded by RNases before entering the cells, and siRNA can also be cleared by renal filtration after intravenous injection [10]. In addition, naked negatively charged siRNA cannot directly penetrate the cell membrane [11]. Therefore, it is of great significance to

* Corresponding author. Department of Radiology, Sun Yat-Sen Memorial Hospital, Sun Yat-Sen University, 510120, China.

E-mail address: wuzhuo@mail.sysu.edu.cn (Z. Wu).

¹ These authors contributed equally to this work.

develop an efficient drug delivery system with good biocompatibility to deliver siRNA to the lesion for HCC treatment.

The advancement of nanotechnology has promoted the development of various drug-loaded nanocarriers. Amylose with excellent characteristics, such as abundant, cheap, good biocompatibility, low toxicity, etc, has been used as a nano-vector for various drugs and gene delivery [12, 13]. Studies showed that amylose-based star polymers could be served as potential siRNA carriers for medical trials [14,15]. Quaternary ammonium cationized amylose (CA) carrier can adsorb negatively charged siRNA on the carrier surface through electrostatic interaction, forming stable nanoparticles (NPs) with gene complex to prevent the degradation of siRNA [16]. In addition, the targeted NPs delivery system can actively deliver therapeutic agents to specific lesions, achieving better treatments. Various targeting ligands have been developed to modify nano-drug delivery carriers, which can actively target tumour blood vessels, matrix microenvironment, or tumour cell surface receptors [17–23]. SP94 peptide (protein sequence: SFSIIHTPLPL) isolated from phage-displayed peptide selections, is a HCC-specific targeting ligand [24]. It can bind to SP94 short peptide-specific receptor GRP78 protein on HCC cell membrane [25,26]. Therefore, the designed drug delivery NPs with SP94 decoration may effectively increase the targeting efficiency of HCC.

The combined use of imaging unit and antineoplastic drugs can simultaneously perform diagnosis, treatment, and treatment response monitoring in an integrated system [27,28]. Magnetic resonance imaging (MRI) can accurately diagnose HCC without invasive biopsy. With the help of MRI contrast agents, radiologists can more clearly distinguish liver lesions, detect relatively small and subtle lesions of tumours, and make an accurate diagnosis [29,30]. The particle size, toxicity, biocompatibility, and degradability of contrast agents are important factors that affect the MRI quality [31]. Superparamagnetic iron oxide NPs (SPIOs) with multi-surface capabilities, high contrast efficiency, and good biocompatibility have been recognized as a most potential MRI contrast in various clinical trials, such as atherosclerotic plaque and tumour imaging [32,33].

Compared to MRI, fluorescence imaging has the advantages of revealing pharmacokinetics and biodistribution throughout body in real time with high sensitivity and specificity, but it suffers from low spatial resolution and poor tissue penetration [34]. Besides, conventional tracking agents, such as fluorescent conjugated polymers, quantum dots, or organic fluorophores, have disadvantages such as poor photostability, significant cytotoxic, and aggregation-caused quenching (ACQ) effect

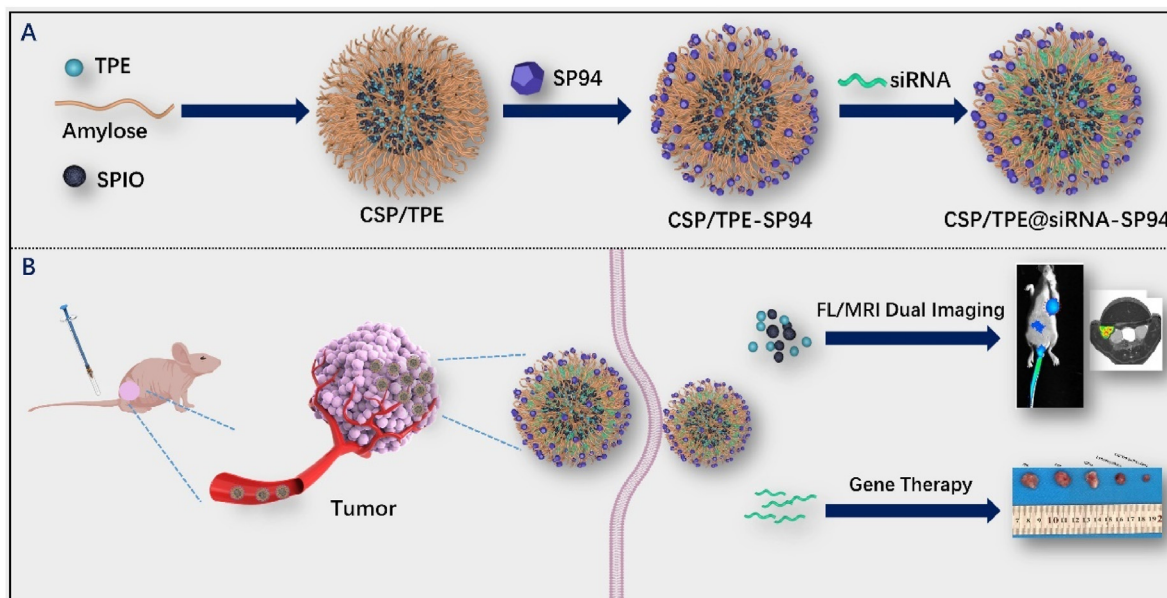
[35]. Aggregation-induced emission (AIE) fluorogens show advantages in terms of low biotoxicity, high brightness, good biodegradability, excellent stability, and facile surface modification [36]. Several studies have reported that AIE fluorophores, such as tetraphenylethylene (TPE) and its derivatives, are widely used as tracking agent to construct multifunctional nano-carrier [37,38]. Therefore, by integrating AIE and SPIOs into a NPs delivery system, dual-modal imaging (fluorescence/MR imaging) can be used to monitor physiological and pathological responses at the cellular level with only one injection.

In this study, we developed a theranostic nanoprobe for HCC-targeted gene therapy, which could deliver siRNA directly to the lesion and monitor the lesion through dual-imaging (fluorescence and MR imaging) modalities. As shown in Scheme 1, CA, SPIO, and TPE were self-assembled to form nanospheres (CSP/TPE). SP94 peptides were decorated on the surface of prepared NPs by amidation reaction, and then survivin siRNA were loaded to CSP/TPE-SP94 NPs. Characterization of physicochemical properties of the prepared NPs was carried out using X-Ray diffraction (XRD), transmission electron microscope (TEM), Zeta potential, gel electrophoresis, fluorescence spectroscopy, thermogravimetric analyzer (TGA), fourier transform infrared (FTIR) spectrometer, vibrating sample magnetometer and MRI scanning. The cytotoxicity of CSP-based NPs was investigated using cell counting kit-8 (CCK-8) and living/dead staining assay. The cellular uptake and distribution of the theranostic NPs against Huh-7 cells were evaluated by confocal laser scanning microscope (CLSM) and flow cytometry. Furthermore, *in vivo* biodistribution and antitumour effect of the prepared nanoparticles were evaluated via Huh-7 tumour-bearing nude mice.

2. Experimental section

2.1. Materials

Amylose (>98%, 83.0 kDa) and glycidyltrimethylammonium chloride (90%, 151.60 Da) were procured from Sigma-Aldrich Co., Ltd. (St Louis, USA). 1-Ethyl-3-(3-dimethylaminopropyl) CSPrbodiimide (98.5%, 191.70 Da) and N-hydroxysuccinimide (98%, 115.09 Da) were purchased from Sigma-Aldrich Co., Ltd. (St Louis, USA). Ferrous chloride ($\text{FeCl}_2 \cdot 4\text{H}_2\text{O}$), 25% ammonia ($\text{NH}_3 \cdot \text{H}_2\text{O}$), ferric chloride ($\text{FeCl}_3 \cdot 6\text{H}_2\text{O}$), acetic acid, Sodium hydroxide (NaOH), and dimethyl sulfoxide (DMSO) were analyzed pure and purchased from Guangzhou chemical reagent factory (Guangzhou, China). Calcein AM, Alexa Fluor 488 Annexin V/



Scheme 1. Schematic illustration of the preparation (A) and application (B) of CSP/TPE@siRNA-SP94

Propidium Iodide (PI) Cell Apoptosis Kit, phosphate buffered saline (PBS, pH 7.4), cell counting kit-8 (CCK8), and One Step TUNEL Apoptosis Assay Kit were procured from Invitrogen Co., Ltd. (Shanghai, China). siRNA epirubicin was obtained from Macklin Biochemical Co., Ltd (Shanghai, China). Fetal bovine serum (FBS), RMPI 1640, trypsin-EDTA, high-glucose Dulbecco's modified Eagle's medium (DMEM), and penicillin-streptomycin were obtained from Gibco Co., Ltd (NY, USA). Dialysis bags (molecular weight cut-off weight: 8000 Da) were bought from Millipore Corporation (USA). Survivin siRNA (sense: 50-CACCG-CAUCUCUACAUUCATT-30; antisense: 50-UGAAUGUAGAGAUGCG-GUGTT-30) were synthesized by GenePharm Co., Ltd. (Shanghai, China). Huh-7 and L02 cells were obtained from Sun Yat-Sen University (Guangdong, China). The cell lines were maintained in DMEM with FBS (10%) and antibiotics (1%) at 37°C, in a humidified 5% CO₂ environment.

2.2. Synthesis of CSP/TPE@siRNA-SP94

2.2.1. Preparation of CA

Amylose (0.50 g) was added to distilled water (25 mL), and pH was adjusted to 12–14 with NaOH solution (4 mol/L) under heating (80 °C). The prepared solution was slowly added 2,3-Epoxypropyltrimethylammonium chloride (0.05 g/mL) and stirred at 50 °C for 12 h. The solution was set to neutral pH value using hydrochloric acid solution after the reactions and then transferred to a dialysis bag (molecular weight cut-off: 8000 Da). The solution was dialyzed against deionized water for two days, then followed by lyophilization to obtain cationic amylose (CA).

2.2.2. Preparation of CSP/TPE

FeCl₃·6H₂O (0.30 g) and FeCl₂·4H₂O (0.15 g) were added to 10 mL of deionized water. The mixture was then neutralized with 1 mol/L sodium hydroxide solution under vigorous stirring at 150°C for 4 h. Oleic acid (0.08 g) and oleylamine (0.08 g) were added to the mixture, and the solution was naturally cooled to room temperature. The obtained mixture was added with a CA solution (0.01 g/mL), stirred at 80 °C for 30 min under nitrogen, then 25% ammonia water (3.0 mL) was added to the solution. After 1 h reaction, the solution was dialyzed against deionized water through a dialysis bag (MWCO:8000) for 48 h. The resulting solution was lyophilized to obtain a composite (CSP) of magnetic NPs modified with quaternary ammonium cationized amylose (CA). TPE powder (4 mg) was dissolved in dichloromethane (4 mL), and then CSP solution (20 mg) was added and mixed well at room temperature, followed by adding pure water (40 mL) while sonicating. After 1 h, the product was put into a dialysis bag (molecular weight cut-off: 2000 Da) and dialyzed with distilled water for 72 h. The dialysate was freeze-dried and stored at 4°C to obtain nanocomposites (CSP/TPE) including of quaternary ammonium cationized amylose, magnetic NPs and TPE.

2.2.3. Preparation of CSP/TPE-SP94

SP94 peptide (5 mg) was dissolved in DMSO (4 mL). N-(3-Dimethylaminopropyl)-N'-ethylcarbodiimide hydrochloride (EDC-HCl) (10 mg) and N-hydroxysuccinimide (NHS) (20 mg) were added into the solution, stirring for 4 h at room temperature in a darkroom to obtain a peptide active ester DMSO solution. Half of the CSP/TPE solution (containing 0.10 g CSP) and acetic acid were added in a round bottom flask, and pH was adjusted to pH5. The peptide active ester solution was then added into the flask, and the reaction was conducted at room temperature for 48 h. The resulting solution was dialyzed (MWCO:8000) against distilled water for 3 days. The sediment was removed by centrifugation of dialysate, and the upper liquid was stored at 4 °C to obtain nanocomposites (CSP/TPE-SP94) including of quaternary ammonium cationized amylose, magnetic NPs, and TPE NPs binding with SP94 peptide.

2.2.4. Preparation of CSP/TPE@siRNA-SP94

CSP/TPE-SP94 was diluted with distilled water at different N/P ratios (molar ratio of CSP/TPE-SP94 nitrogen to siRNA phosphorus), and then

mixed with 2 pmol/μL siRNA solution. The solution was mixed for 10 s and kept for 25 min at room temperature to form nanocomposites (CSP@siRNA/TPE-SP94).

2.2.5. Characterization of various CSP-based NPs

A Nano ZS90 analyzer (Malvern Instruments Ltd, UK) with a 4 mW He-Ne laser (633 nm) was used to determine the size, size distribution, polydispersity, and surface charge of the prepared NPs at room temperature. The morphology of micelles with or without TPE encapsulating was observed by TEM (JEOL JEM-2010F, Japan) at room temperature. Briefly, a sample was stained using 2% (w/v) phosphotungstic acid, transferred onto a copper grid, air-dried and imaged. The infrared spectra of CSP NPs in the range of 4000–399 cm⁻¹ was measured by FTIR. A series of CSP/TPE acetonitrile/water composite micelle solutions were prepared according to the TPE concentration gradient and tested using a fluorescence spectrophotometer with an excitation wavelength of 350 nm (Hitachi F-7000, Hitachi, Japan).

2.2.6. siRNA condensation assay and siRNA release profile

To investigate siRNA condensation ability of CSP/TPE@siRNA, agarose gel electrophoresis was used. CSP/TPE@siRNA at different N/P ratios (7.5 μL) with loading buffer (2.5 μL) were mixed at room temperature. Then, the mixture was run on agarose gel (1% (w/v)) containing ethidium bromide (1.0 mg/mL) in Tris-acetate-EDTA (TAE) buffer solution (pH 8.0) at 4 V for 4 h. The gel image of siRNA bands was recorded using a Dolphin-Doc Molecular Imaging System (Wealtec, USA).

The release curve of siRNA was obtained as follows. Briefly, CSP/TPE@siRNA-SP94 aqueous solution (1.5 mg/mL) was placed in a centrifuge set containing 15 mL of buffer solution following the manufacturer's protocol (Amicon® Ultra-15-100 kDa, Sigma-Aldrich). The centrifugal tube with the filter was placed in a shaker at 100 rpm and 37 °C. At fixed time points, a sample solution (1 mL) was collected and replaced with equal amount of fresh buffer. The released siRNA amount was acquired through high performance liquid chromatography (HPLC). The cumulative release (%) was evaluated according to the following formula: $Cumulative\ release\ (\%) = \frac{C_n \cdot V + \sum_{i=1}^{n-1} C_{n-1} \cdot V_i}{M_0} \times 100\%$

Herein, C_n is siRNA concentration measured at each time point, V is experimental sample solution volume; V_x is sampling volume at each time point, and M₀ is the total amount of siRNA in the sample.

2.3. Gene transfection in vitro

Huh-7 cells were seeded in a 24-well plate (density: 1 × 10⁵ cells/well) and incubated at 37°C for 24 h in a 5% CO₂ atmosphere. The prepared CSP-based NPs were mixed with FAM-labelled siRNA (2.0 μg) at N/P ratios of 8, 10, 20, and 30 for 30 min, then added to the plate. The prepared NPs were co-cultured with Huh-7 cells for 6 h, and then washed with fresh DEME medium containing 10% serum. The ability of prepared NPs to deliver FAM-siRNA to Huh-7 cells was investigated using a fluorescence microscopy (Hitachi F-7000, Hitachi, Japan).

2.4. In vitro MRI test

A series samples of CSP/TPE@siRNA-SP94 were prepared, and the SPIONs concentration in the samples was set to 0.01, 0.02, 0.04, 0.09, 0.19, 0.36, 0.72, 1.43 mM, respectively. A sample of 1.5 mL was transferred to a transparent rigid plastic centrifuge tube (2 mL) and placed on a foam plate. The prepared samples were scanned by a 1.5T MRI scanner (Intera 1.5T MR Systems, Koninklijke Philips N.V.) at room temperature. Scan sequence included T2*-weighted imaging and T2-mapping. T2*-weighted imaging parameters were: repetition time (TR) = 2600 ms, echo time (TE) = 100 ms, flip angle = 90°, acquisition matrix = 384 × 305, NA (Number of acquisitions) = 6, field of view (FOV) = 80 mm × 80 mm, slice gap = 2 mm and slice thickness = 2 mm. T2 mapping was performed using a single-layer, multi-echo selectable echo sequence

scanning whose parameters were: TE = 0, 20, 40, 60, 80, 100, 120, 140, 160 ms; TR = 1500 ms; acquisition matrix = 176 × 123; FOV = 80 mm × 80 mm; NA = 3; slice gap = 1.5 mm; slice thickness = 1.5 mm.

2.5. *In vitro* evaluation of antitumour effects

The cytotoxicity of the nanocomplex to Huh-7 cells was investigated by CCK8 assay. Briefly, cells in DMEM containing 10% (v/v) fetal bovine serum (FBS) were incubated at 37 °C for 48 h. The cells were then seeded in a 96-well plate with a density of 1.0×10^6 cells per well and incubated for 24 h. After replacing of DMEM with fresh medium, Huh-7 cells were treated with different concentrations of siRNA, CSP/TPE@siRNA and CSP/TPE@siRNA-SP94. Huh-7 cells treated with free PBS were used as the control group. After incubating at 37 °C for 48 h, the CCK8 reagent (10 mg/mL) was added to each well and the treated cells were incubated for 4 h. The optical densities (OD) of each group were measured at 490 nm using a Fluoroskan microtiter plate reader (Thermo Scientific, USA).

The formula for determining cell viability was: cell viability =

$$\frac{\text{sample OD value} - \text{blank OD value}}{\text{control OD value} - \text{blank OD value}} \times 100\%$$

To study the effect of the prepared NPs on cellular uptake, Huh-7 cells were cultured in a 12-well plate (4×10^4 cells/well) followed by incubation for at 37 °C 12 h. The cells were then co-cultured with CSP/TPE@siRNA and CSP/TPE@siRNA-SP94 NPs, respectively. Each group contained 40 nM siRNA. At selected time points, the treated cells were washed thrice using PBS buffer and trypsinized for the flow cytometry analysis. The harvested cells were resuspended in fresh medium, washed with PBS, and then resuspended in 1.0 mL PBS buffer. The cells were analyzed using a FACS calibur flow cytometer (Beckman Dickinson, San Jose, CA). Confocal fluorescence microscopy (CLSM) (Carl Zeiss LSM 710, Carl Zeiss Microscopy, Jena, Germany) was used to evaluate the cellular uptake of the prepared NPs. The cells (1×10^5 cells per well) were then co-cultured with CSP/TPE@siRNA and CSP/TPE@siRNA-SP94 NPs, respectively. Each group contained 40 nM siRNA. At selected time points, the treated cells were washed thrice using PBS and fixed in paraformaldehyde (4% in PBS) for 15 min prior to CLSM imaging. The Cell nuclei were stained using 4',6-diamidino-2-phenylindole (DAPI).

2.6. *In vivo* evaluation of antitumour effects and MRI study

2.6.1. Animals and tumour bearing model

Male BALB/c nude mice (aged 6 weeks, 19–23 g) were bought from animal centre of Sun Yat-Sen University (Guangdong, China). The animal experiment (No. SYSU-IACUC-2020-000048) was approved by the Laboratory Animal Ethics Committee Sun Yat-Sen University (Guangdong, China). Animal treatment and handling were carried out in accordance with the National Institutes of Health Guide for Care and Use of Laboratory Animals. Nude mice were placed in cages (5 per cage) and provided with standard water as well as mouse chow. Harvested Huh-7 cells (4×10^6 cells per 100 μL PBS) were implanted into the right leg area of mice by subcutaneous injection. The tumour size was monitored, and the tumour volumes determined as:

$$\text{Tumour volume} = [(\text{tumour length}) \times (\text{tumour width})^2]/2.$$

2.6.2. *In vivo* imaging and biodistribution analyses

When the tumour volume reached 100–200 mm³, the nude mice were randomized into 2 groups (n = 5). Two groups of mice were injected with 100 μL of CSP/TPE@siRNA (1 mg/mL) and CSP/TPE@siRNA-SP94 NPs (1 mg/mL) via the tail veins, respectively. Fluorescence images and the semi-quantitative results of TPE at 1 h, 6 h, 12 h, and 24 h were obtained after intravenous administration utilizing *in vivo* imaging system (In vivo Xtreme, Bruker, Germany). The TPE signal was obtained at an excitation and filter wavelengths of 523 nm and 560 nm, respectively. The mice were sacrificed 24 h after injection. The major organs (liver, heart, spleen, kidneys, lung) and tumours were removed for imaging and

biodistribution analysis.

A 3.0T MRI scanner (Ingenia 3.0T MR Systems, Koninklijke Philips N.V.) with a customized rodent coil was used to scan Huh-7 tumour-bearing mice. The experimental mice were anesthetized using a 4% isoflurane/air mixture administered via a nose cone. Their body temperature was maintained at 37 °C. The mice were divided into 2 groups (n = 5). Two groups of mice were injected with 100 μL of CSP/TPE@siRNA (1 mg/mL) and CSP/TPE@siRNA-SP94 NPs (1 mg/mL) via the tail veins, respectively. Then, they were subjected to MRI scanning with fast spin-echo T2*-weighted imaging and T2-mapping sequence at different time points (pre-injection, 6 h after injection, 12 h after injection, and 24 h after injection). For the fast spin-echo T2*-weighted imaging, imaging parameters were: TR = 1600 ms, TE = 60 ms, NA = 3, acquisition matrix = 254 × 254, FOV = 128 mm × 128 mm, slice thickness = 1 mm, flip angle = 90°, slice gap = 1 mm. T2-mapping was performed using single-slice as well as multi-echo spin-echo sequence with scan parameters as: TR = 1400 ms, TE = 25, 50, 75, 100 ms, acquisition matrix = 109 × 108, NA = 3, FOV = 128 mm × 128 mm, slice gap = 1.5 mm, slice thickness = 1.5 mm. At each time point, MR images and their equivalent MRI signal intensities were recorded, then calculated.

2.6.3. Therapeutic analysis

Antitumour effects of the prepared NPs were evaluated using nude mice with Huh-7 tumours. The tumour-bearing mice were randomly assigned into 5 groups (n = 5): PBS, CSP/TPE, free siRNA, CSP@siRNA, and CSP@siRNA-SP94. The mice were received 100 μL of therapeutic agents: PBS, CSP/TPE (1000 mg/mL), free siRNA (40 nM), CSP/TPE@siRNA (containing 40 nM siRNA) and CSP/TPE @siRNA-SP94 (containing 40 nM siRNA @100 μL) via the tail vein every other day. The tumour volumes, body weight, and survival rate of mice were recorded every other day. After 14 days of treatment, the experimental mice were sacrificed. Their major organs were resected, fixed with 4% paraformaldehyde and sliced for hematoxylin and eosin (H&E) staining. For the survival rate analysis, Huh-7 tumor bearing mice were treated under the same conditions up to a period of 40 days, and the number of surviving mice in each group was recorded.

2.6.4. Statistical analysis

Data were shown as mean ± SD. The students' t-test was used to compare statistical differences between two groups, while one-way ANOVA was used to compare multiple groups. $p \leq 0.05$ (*) was considered significant, while $p \leq 0.01$ (**) was considered very significant.

3. Results and discussion

3.1. Characterizations of the prepared CSP nanoparticles

The prepared NPs were assembled using CA, SPIO, TPE, survivin siRNA, and SP94 peptide to achieve HCC-targeted gene therapy and dual-mode imaging functions. The hydrophobic SPIO NPs were synthesized [39], and TPE was added into the inner core of SPIO NPs through physical entrapment via hydrophobic interactions. Therefore, CSP could integrate a large amount of hydrophobic TPE and SPIO in the core, while maintaining water solubility by using the hydrophilic outer shell layer of CA. The TEM images showed that SPIO NPs were black dots with an average size of 5–8 nm (Fig. 1a and d). Both CSP and CSP/TPE@siRNA-SP94 NPs showed similar spherical shape with an average size of 155 ± 2.8 nm (Fig. 1b and e) and 178 ± 0.5 nm (Fig. 1c and f), respectively. The PDI of CSP and CSP/TPE@siRNA-SP94 NPs were 0.18 and 0.25, respectively. The size of NPs ranged from 100 nm to 200 nm is optimal for enhanced permeability and retention (EPR) effects [40]. Previous works had proved that nano-scaled drug carriers are easily internalized by tumour cells and can penetrate deeper into tumour tissues for therapy [32]. The surface potential of CSP/TPE and CSP/TPE@siRNA-SP94 was 23.5 ± 1.7 mV and 5.8 ± 0.6 mV,

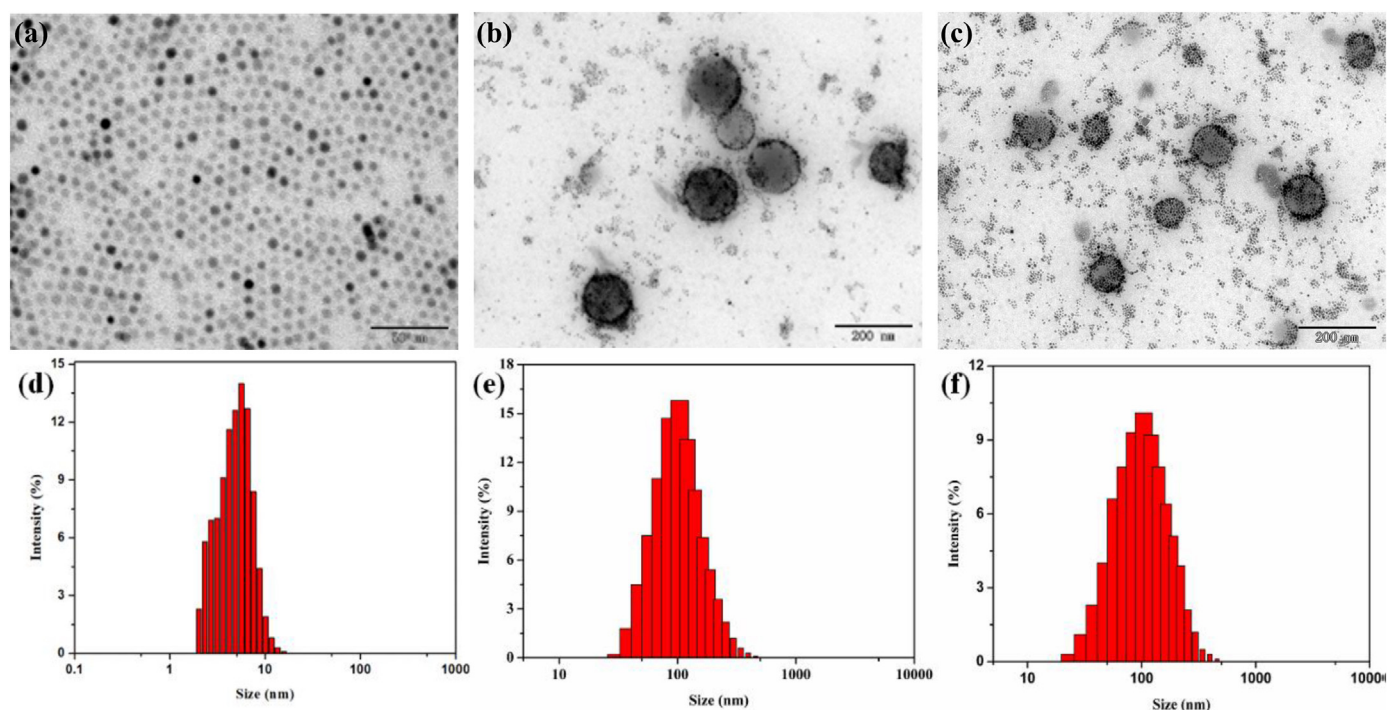


Fig. 1. Characterization of the prepared NPs: TEM images of SPIO (a), CSP(b), and CSP/TPE@siRNA-SP94(c), size distribution profiles of SPIO(d), CSP(e) and CSP/TPE@siRNA-SP94(f).

respectively, indicating that the negatively charged siRNA was successful adsorbed into the core of CSP/TPE@siRNA-SP94.

The infrared spectrum of SPIO NPs was shown in Fig. 2a. The peaks at 560.0 cm^{-1} were the stretching vibration absorption peaks of metal and oxygen atoms. The two peaks at 1570 cm^{-1} corresponded to the symmetric stretching vibration and antisymmetric stretching vibration peaks

of $\text{C}=\text{O}$, which were characteristic peaks of carboxylate. The two peaks at 2920 cm^{-1} and 2850 cm^{-1} corresponded to C–H stretching vibration absorption peaks in the oleic acid molecule. The photoluminescence (PL) intensity of CSP/TPE ($25\text{--}1000\text{ }\mu\text{g/mL}$) was shown in Fig. 2b, and the optimal concentration range of TPE was $100\text{--}800\text{ }\mu\text{g/mL}$. The maximum fluorescence intensity around 450 nm indicated that TPE had been

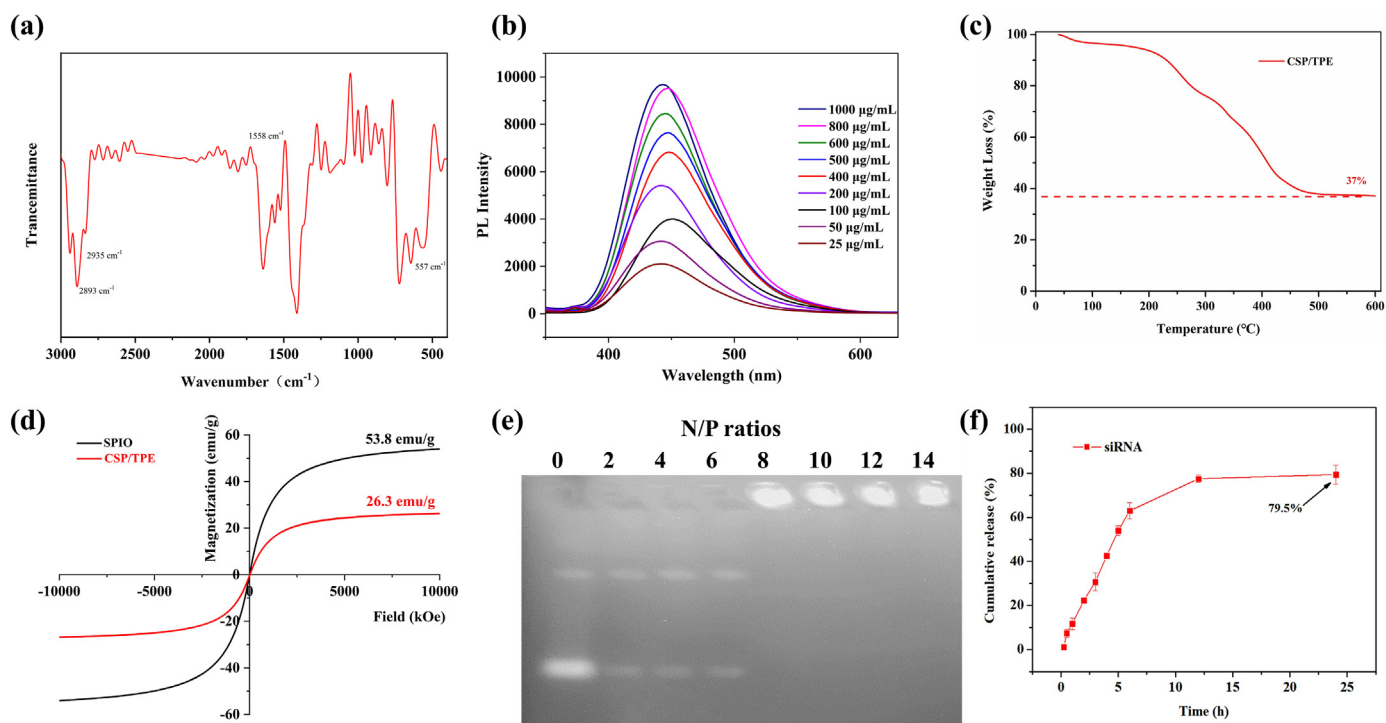


Fig. 2. (a) FTIR spectrum of SPIO; (b) PL spectra of CSP/TPE; (c) TG curves of CSP/TPE; (d) Magnetization curve of SPIO and CSP/TPE; (e) Agarose gel electrophoresis of CSP/TPE with survivin siRNA at N/P ratios of 0, 2:1, 4:1, 6:1, 8:1, 10:1, 12:1, 14:1; (f) *in vitro* siRNA release from CSP/TPE@siRNA-SP94 at pH7.4.

successfully introduced into CSP NPs. When the concentration of TPE decreased, the solubility of TPE increased and the fluorescence intensity became weaker. When the concentration of TPE increased, the solubility of TPE decreased, forming an aggregate state. Therefore, the AIE fluorescence intensity enhanced. Fig. 2c showed the thermogravimetric curve of CSP/TPE NPs between 40 °C and 700 °C. The final mass loss of CSP/TPE was 63%, indicating the content of SPIO was 37%. Due to the addition of SPIO, the content of thermally degradable components in CSP/TPE was reduced, suggesting SPIO has been successfully introduced into CSP/TPE. The magnetic response of magnetic materials is an important index for evaluating magnetic materials. Fig. 2d showed the hysteresis loops of SPIO and CSP/TPE NPs at 300 K. In the cyclic scanning of applied magnetic field from - 20,000 OE to 20,000 OE, when the applied magnetic field intensity was zero, the residual magnetization of SPIO or CSP/TPE became zero. This result indicated that both SPIO and CSP/TPE had superparamagnetism. The saturation magnetization of SPIO and CSP/TPE NPs were 53.8 emu/g and 26.3 emu/g, respectively. The reason for the decrease in saturation magnetization of CSP was that CA was coated on the surface of SPIO, leading to a decrease in magnetization. As CSP/TPE still showed an excellent magnetic response to the external magnetic field, it could be applied for subsequent MRI scans. The condensation ability of CSP/TPE nanocomplex was investigated as the prepared drug carriers could condense genes into NPs of appropriate size, thereby enhancing the cellular uptake. The condensation ability of prepared NPs to survivin siRNA was evaluated using electrophoretic mobility of the prepared CSP/TPE@siRNA-SP94 at various N/P ratios on the agarose gel. As shown in Fig. 2e, the prepared NPs gene carrier could efficiently and completely condense siRNA at N/P ratios of 8 (Fig. 2e). We further investigated the release behavior of survivin siRNA from CSP/TPE@siRNA-SP94. The prepared NPs released 50.0% survivin siRNA at 37 °C for the first 5 h, and then reached to 79.8% at 24 h (Fig. 2f).

Fig. 3 showed the fluorescence picture of cells treated with CSP/TPE@FAM-siRNA and CSP/TPE@FAM-siRNA-SP94 at various N/P ratios. These images indicated that the prepared NPs had the ability to transfer siRNA into cells. The transfection efficiency of CSP/TPE@siRNA-SP94 as a gene encapsulation vector was N/P ratio dependent within certain range (NP ratio of 8–20). When the N/P ratio was set to 20, CSP/TPE@siRNA-SP94 showed the best gene transfection efficiency compared with the other groups. At the same NP ratio (8, 10 or 20) condition, CSP/TPE@siRNA-SP94 showed a higher transfection efficiency compared to that of CSP/TPE@siRNA.

The results of MRI T_2 -weighted imaging for CSP/TPE@siRNA-SP94 NPs. T_2 -weighted imaging was obtained by conventional spin echo SE sequence scanning, with pulse repetition interval time TR = 1500 ms, echo time TE = 96.191, 167.98, 293.32, 487.83, 752.57, 1032.6,

1259.3, 1430.2 ms, FS = 1.5. With the increase of Fe concentration, the MR image gradually darkened (Fig. 4a). The concentration of Fe (mM) was plotted with reciprocal R_2 (s^{-1}) of T_2 relaxation time (Fig. 4b). The specific relaxivity value was determined to be $31.9 \text{ Mm}^{-1}\text{s}^{-1}$ for CSP/TPE@siRNA-SP94 NPs and $53.0 \text{ Mm}^{-1}\text{s}^{-1}$ for SPIOs, respectively. This result suggested that the prepared CSP/TPE@siRNA-SP94 NPs could achieve MRI performance, and R_2 value was similar to other SPIOs [41, 42].

3.2. Cytotoxicity assays in vitro

The cytotoxicity of CSP-based NPs was investigated using CCK8 assay. As shown in Fig. 5a, when the concentration of CSP/TPE and CSP/

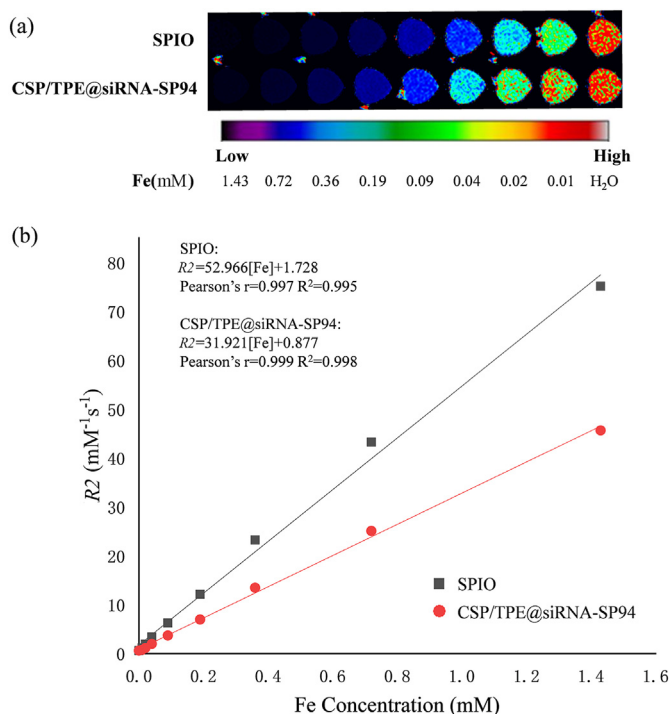


Fig. 4. *In vitro* MRI properties of CSP/TPE@siRNA-SP94: (a) *In vitro* T_2 -weighted MR image of CSP/TPE@siRNA-SP94 and SPIO at different concentrations; (b) Plot of the transverse relaxivity (R_2) of CSP/TPE@siRNA-SP94 and SPIO.

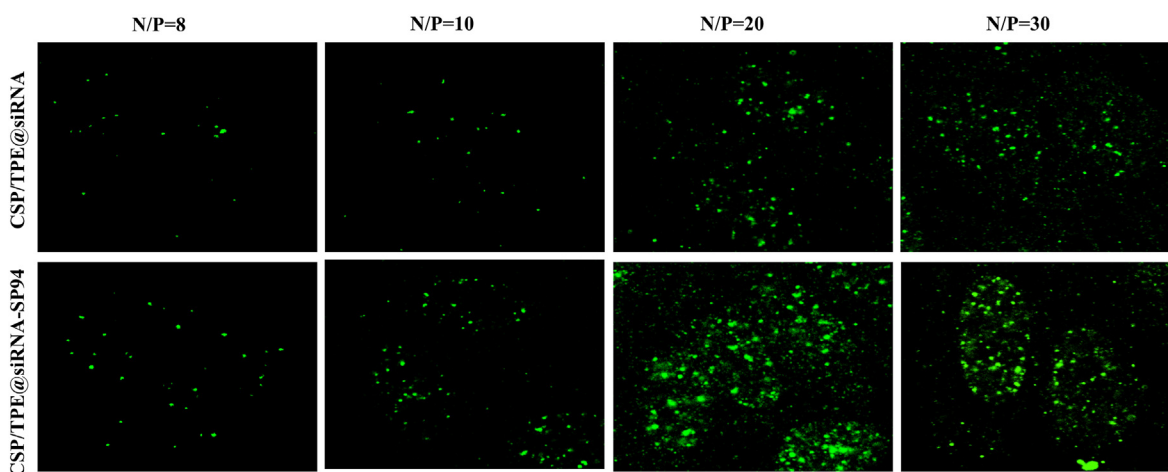


Fig. 3. Transfection efficiencies in Huh-7 cells. Fluorescence microscopy images of Huh-7 cells transfected by CSP/TPE@FAM-siRNA and CSP/TPE@FAM-siRNA-SP94 after 48 h at the N/P ratios 8, 10, 20, and 30.

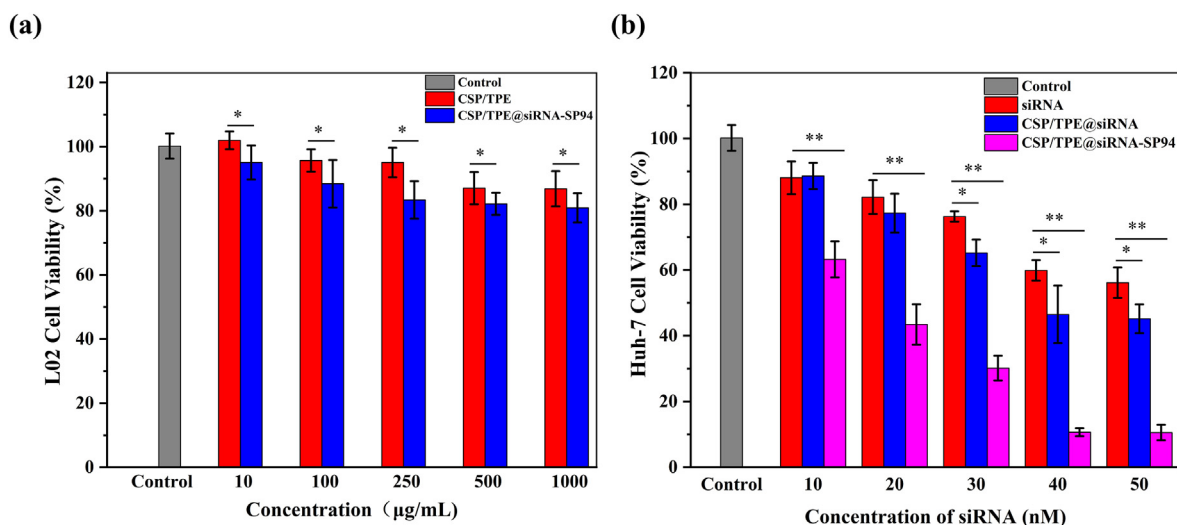


Fig. 5. Cytotoxicity of cells treated with the prepared CSP-based NPs. (a) CCK-8 results of CSP and CSP/TPE co-cultured with L02 cells at various concentrations; (b) CCK-8 results of CSP/TPE@siRNA and CSP/TPE@siRNA-SP94 co-cultured with Huh-7 cells at various concentrations.

TPE@siRNA-SP94 ranged from 10 to 1000 µg mL⁻¹, cell viability was above 80%, indicating CSP/TPE and CSP/TPE NPs had good biocompatibilities toward L02 cells. For Huh-7 cells, when the siRNA concentration ranged from 0 to 40 nM, the higher the siRNA concentration in the prepared CSP-based NPs, the stronger the anti-tumor effect. The naked siRNA at the range of (0–30 nM) showed a little effect on cytotoxicity, as the cell viability of siRNA group was about 80–90%. Under the same siRNA concentration range (0–40 nM), the cell viability of the

targeted NPs (CSP/TPE@siRNA-SP94) was much lower than that of the non-targeted group CSP/TPE@siRNA. This might be due to the fact that SP94 could target to HCC cells, thereby enhancing the accumulation of survivin siRNA in HCC cells.

The live/dead staining assay showed similar findings to these of CCK8 (Fig. 6a and b). The image of cells cultured with CSP/TPE showed a few red fluorescence signals (dead cells), indicating CSP/TPE had good biocompatibility to cells. The images of cells cultured with CSP/

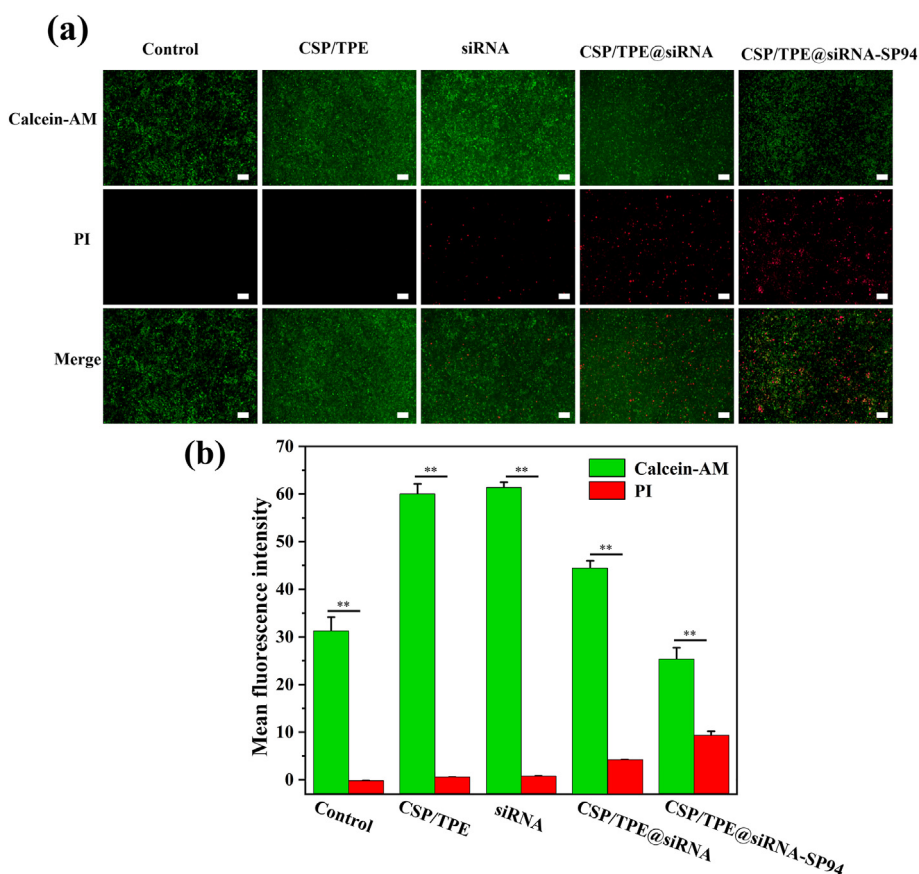


Fig. 6. Dead/live cell staining results of control, CSP/TPE, siRNA, CSP/TPE@siRNA and CSP/TPE@siRNA-SP94 groups cocultured with Huh-7 cells (a). The mean fluorescence intensity of cells treated with control, CSP/TPE, siRNA, CSP/TPE@siRNA and CSP/TPE@siRNA-SP94 groups (b).

TPE@siRNA or CSP/TPE@siRNA-SP94 showed a large amount of red fluorescence signals, indicating they had good inhibitory effects on the Huh-7 cells. To investigate the inhibitory mechanisms of survivin siRNA on Huh-7 cells, Western blotting (WB) was used to evaluate protein expression level of caspase-3 and survivin in Huh-7 cells, respectively. Our results showed that after 48 h, expression level of caspase-3 was considerably up-regulated in the groups of Huh-7 cells treated with CSP/TPE@siRNA and CSP/TPE@siRNA-SP94 (supplemental data Fig. S4). Caspase-3 plays an irreplaceable role in cell apoptosis. Overexpression of caspase-3 indicated that CSP/TPE@siRNA-SP94 could effectively induced the apoptosis of Huh-7 cells. Moreover, the expression level of survivin was suppressed in the groups of Huh-7 cells treated with CSP/TPE@siRNA and CSP/TPE@siRNA-SP94. This result suggested that CSP/TPE@siRNA-SP94 NPs could effectively delivery survivin siRNA, inhibiting the growth of Huh-7 cells.

3.3. Cellular uptake in vitro

Intracellular distributions of CSP-base NPs in cells were investigated using confocal laser scanning microscopy (CLSM). Compared with CSP/TPE@siRNA group, the targeting group CSP/TPE@siRNA-SP94 showed much stronger red fluorescence (Fig. 7a and b). This finding indicated that under the same conditions, Huh-7 cells would intake more CSP/TPE@siRNA-SP94 NPs than CSP/TPE@siRNA NPs. The enhanced accumulation of NPs indicates that the targeted NPs could preferentially accumulate in the cytoplasm through receptor-mediated endocytosis effect. Furthermore, the difference in fluorescence intensity between SP94-targeted NPs and nontargeted NPs expanded after 12 h incubation (Fig. 7c). This was due to the fact that the targeting effect of SP94 peptide promote the cell uptake more targeted NPs within 12 h. The fluorescence flow cytometer results at 4 h (Figs. 7d) and 12 h (Fig. 7e) also showed the active targeting effect of SP94 peptide. In addition to the ability of SP94 to facilitate receptor-mediated cellular uptake, the cationic surface of CSP/TPE@siRNA-SP94 helped them to tightly connect with anionic cell membranes through non-specific electrostatic interactions. NPs can enter mammalian cells by endocytosis [43], then from membrane-bound

vesicles and enwrap NPs to be internalized.

3.4. In vivo evaluation of antitumour effects and MRI study

To investigate whether CSP-based NPs were suitable for imaging *in vivo*, BALB/c mice xenografted with Huh-7 tumour were injected intravenously with 1 mg mL^{-1} of CSP/TPE@siRNA and CSP/TPE@siRNA-SP94 NPs. As shown in Fig. 8a, CSP/TPE@siRNA and CSP/TPE@siRNA-SP94 had good *in vivo* imaging ability for Huh-7 tumor. The experimental mice were sacrificed 24 h after injection to examine the distribution of CSP/TPE@siRNA and CSP/TPE@siRNA-SP94 in tumours as well as major organs (Fig. 8b). The prepared NPs flowed in the circulatory system of mice and mainly accumulated in the liver and tumours. This might be due to the metabolic function of animals. The results of mean fluorescence intensity of the tumor indicated that the AIE fluorescence intensity values of CSP/TPE@siRNA and CSP/TPE@siRNA-SP94 NPs were above 200 a.u at 1 h and 6 h of post-injection. The fluorescence intensities of the CSP/TPE@siRNA-SP94 NPs observed at 12 h and 24 h of post-injection were 1.7 and 3.3 times higher than that of CSP/TPE@siRNA NPs at the same time points, respectively (Fig. 8c). This result suggested CSP/TPE@siRNA-SP94 with SP94 guidance could accumulate in tumor area more effectively than CSP/TPE@siRNA NPs.

As SPIO could generate T_2 -weighted imaging signal intensity, the Huh-7 tumour-targeting ability of CSP/TPE@siRNA-SP94 could be monitored noninvasively through MRI scan. We evaluated the imaging quality of MRI *in vivo* through a mouse model. Mice were scanned before the injection of CSP/TPE@siRNA or CSP/TPE@siRNA-SP94 NPs. After each mouse was injected with the prepared nano-drug carrier, the scans were done at various time points, i.e., pre-injection, post 6 h injection, post 12 h injection, and post 24 h injection. Representative scan images of tumour sections were obtained at different time points (Fig. 8d). After administration of CSP/TPE@siRNA-SP94 NPs, the normalized MR signal intensity values and T_2 value of tumour region of interest were remarkable reduced at post 6 h injection and post 12 h injection. After administration of CSP/TPE, there was little difference between normalized MR signal intensity and T_2 values observed in Huh-7 tumours. The

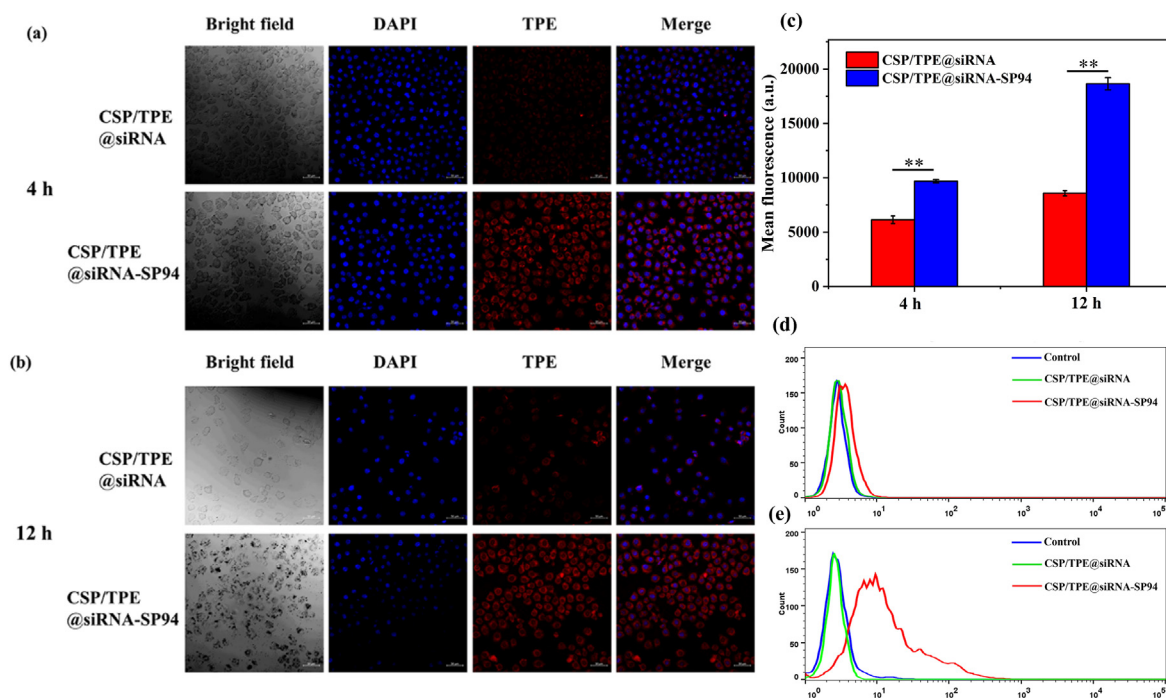


Fig. 7. Intracellular uptake of CSP/TPE@siRNA and CSP/TPE@siRNA-SP94 NPs by Huh-7 cells. The CLSM images of cells incubated with the prepared NPs at 4 h and 12 h were shown in panels (a) and (b), panel (c) showed the mean fluorescence of the prepared NPs co-cultured with Huh-7 cells at 4 h and 12 h. Flow cytometer results of the fluorescence at 4 h and 12 h were shown in panels (d) and (e), respectively.

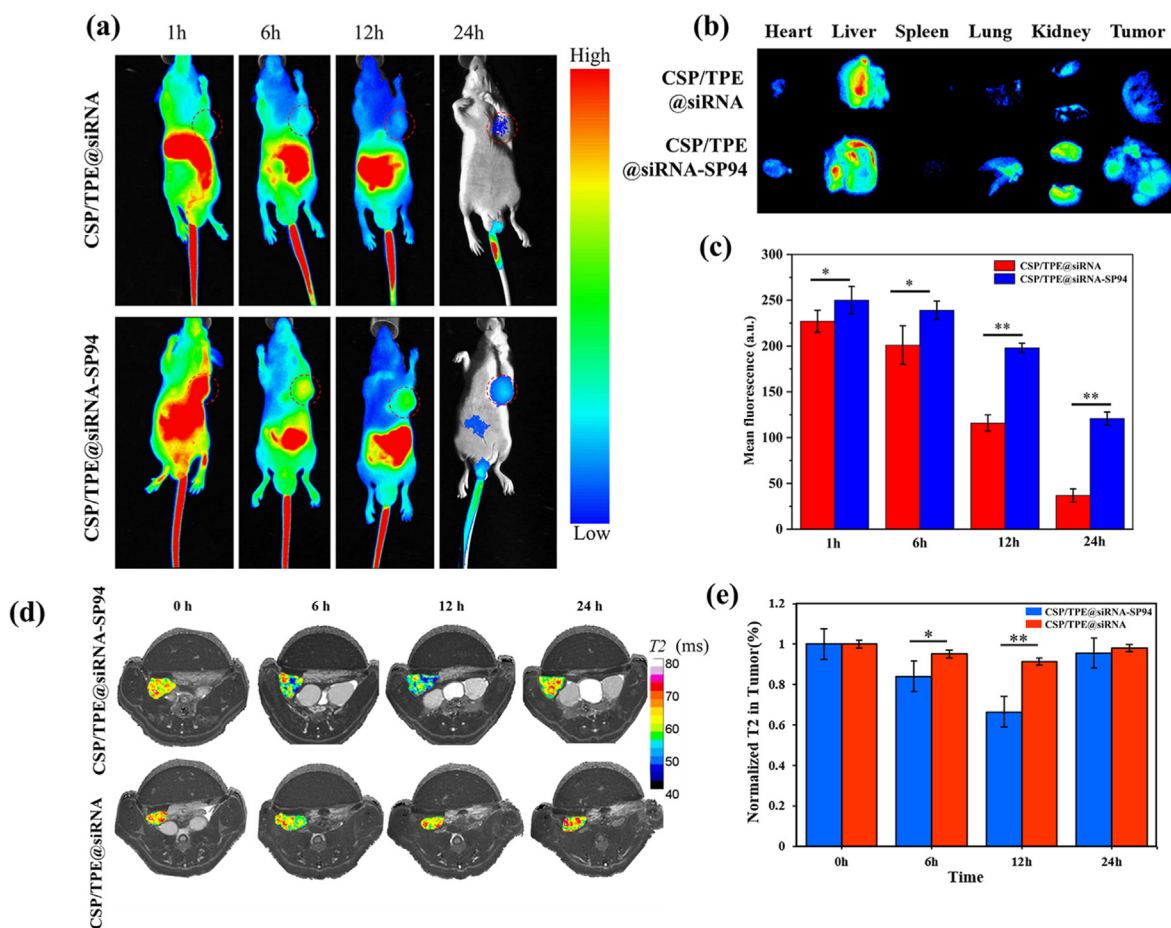


Fig. 8. Fluorescence/MRI dual-modality imaging of the prepared NPs *in vivo*. (a) *In vivo* fluorescence images of Huh-7 tumour-bearing nude mice after injection with CSP/TPE@siRNA and CSP/TPE@siRNA-SP94 at different time points; (b) *Ex vivo* fluorescence images of major organs and tumours dissected from mice at 24 h post-injection; (c) Mean *in vivo* fluorescence signal intensity of the tumor area at different time points; (d) *In vivo* MR images of Huh-7 tumour-bearing nude mice before and after injection with CSP/TPE@siRNA and CSP/TPE@siRNA-SP94 at different time points; (e) T2 signal intensity analysis of T2 reduction in tumours (*: $p < 0.05$; **: $p < 0.01$).

T2 value of tumour region of interest in CSP/TPE group decreased by 5% at 6 h and 9% at 12 h after injection, respectively; while for the CSP/TPE@siRNA-SP94 group, T2 were decreased by 2% at 6 h and 34% at 12 h after injection, respectively. The T2 value of CSP/TPE@siRNA and CSP/TPE@siRNA-SP94 group decreased to 16% and 4%, ($P > 0.05$) respectively, at post 24 h injection (Fig. 8e). The lower the T2 value, the better the targeted imaging effects. This result corresponded with the finding that SP94-modified nanocarriers exhibited higher targeting ability to Huh-7 cells (Figs. 5–7). The inhomogeneous distribution of low signal intensity on T2-weighted images reflects tumour heterogeneity, and the patchy T2 hypointensity inside the tumour may correspond to more active tumour cells or well-perfused regions [44].

The antitumour effect of CSP *in vivo* was investigated in Huh-7 tumour bearing nude mice (Fig. 9). The results showed that tumours treated with PBS and naked surviving siRNA had rapid tumour growth, on the 14th day with an averaged tumour size of 1823, 1599 mm³, respectively. Meanwhile, the tumours treated with CSP/TPE NPs and CSP/TPE@siRNA were suppressed with an averaged tumour size of 889 and 502 mm³, respectively. The tumour growth was considerably suppressed by CSP/TPE@siRNA-SP94 NPs with an averaged tumour size of 240 mm³ on the 14th day. This result indicated that the prepared gene delivery nanoplatform CSP/TPE@siRNA-SP94 NPs could effectively release siRNA at the lesion area and exert an excellent anti-tumor effect, when compared to the other groups. Changes in mice body weight were monitored to evaluate treatment-associated toxicity (Fig. 9c). The body weight of nude mice with Huh-7 tumours in all NPs treated groups was

not much different from that of the PBS control group. In addition, the survival rate assay suggested that CSP/TPE@siRNA-SP94 showed the best anticancer effect, compared to the other groups (Fig. 9d). H&E staining results of major organs showed that all the prepared CSP-based NPs had good histocompatibility (Fig. 9e). Therefore, CSP/TPE@siRNA-SP94 treatment combined with controllable siRNA release, dual-modal real-time tracing and gene therapy could achieve a more ideal anti-tumour therapy strategy with low side effects.

5. Conclusion

We successfully prepared a theranostic nanoplatform CSP/TPE@siRNA-SP94 for liver cancer therapy. The experiments results showed that the prepared CSP/TPE@siRNA-SP94 NPs were spherical with an average size of 178 ± 0.5 nm, and the surface potential of CSP/TPE@siRNA-SP94 5.8 ± 0.6 mV. *In vitro* gel and transfection assays indicated that siRNA could be efficiently condensed into the prepared NPs system and showed high transfection efficiency at an NP ratio of 20. Dual-imaging modal (fluorescence and MRI) of the NPs was tested *in vitro* and *in vivo*, showing enhanced imaging properties. This result indicated that the prepared NPs might be a potential diagnosing tool in clinical applications. Cytotoxicity assays (CCK8 and live & dead cell staining) showed CSP/TPE@siRNA-SP94 could remarkably inhibited the proliferation of Huh-7 cells. The results of cellular uptake *in vitro* and bio-distribution *in vivo* indicated that CSP/TPE@siRNA-SP94 with the modification of SP94 (HCC-targeting NPs), could be more effectively

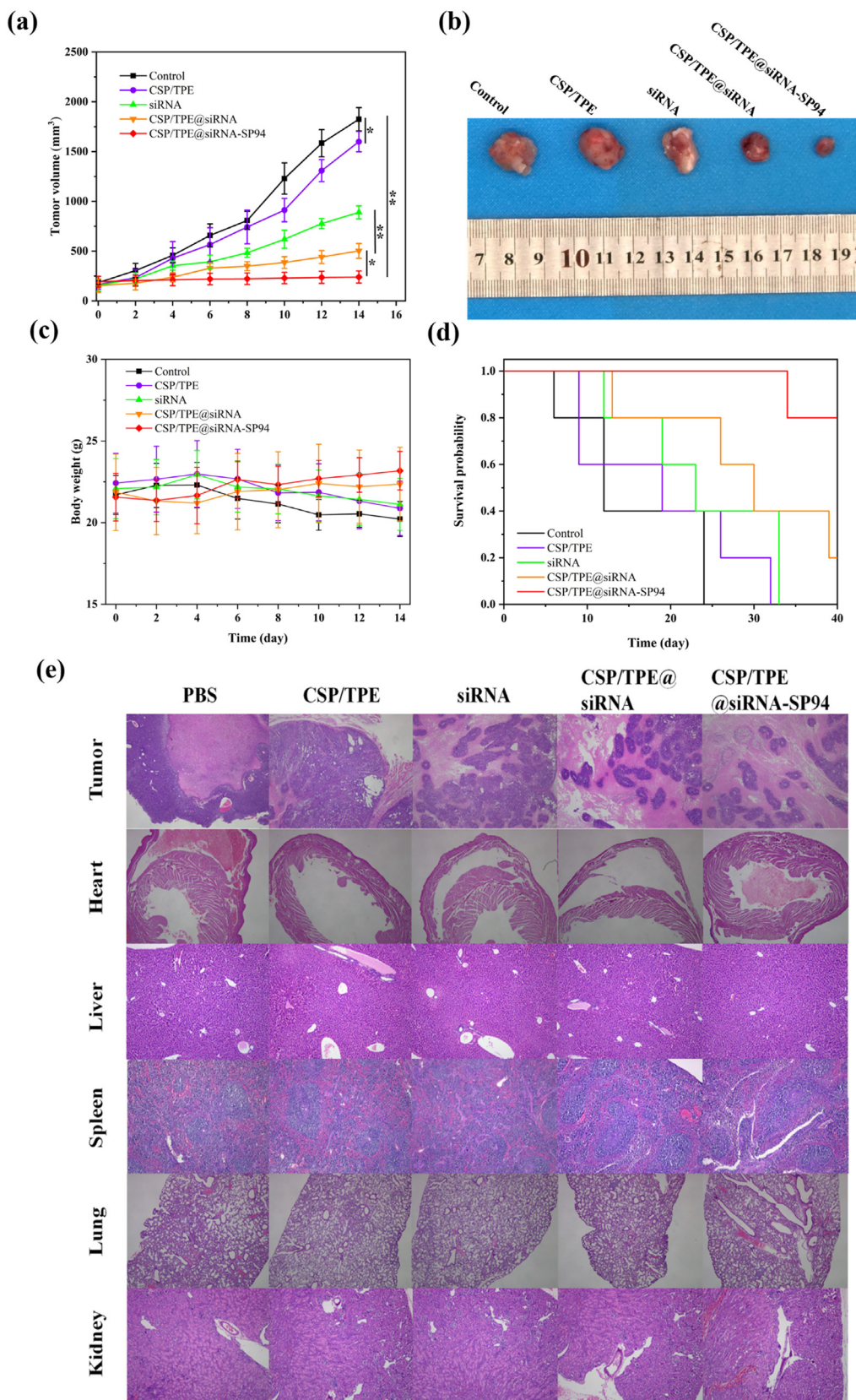


Fig. 9. Antitumour effect of CSP *in vivo*. The tumour-bearing mice were received 100 μ L of therapeutic agent (PBS, CSP/TPE, siRNA, CSP/TPE@siRNA, CSP/TPE@siRNA-SP94) via the tail vein every other day. (a) Plot of tumour volume over 14 days; (b) Image of dissected tumours from the mice after final injection on day 14; (c) Plot of tumour-bearing mice weight over 14 days; (d) Survival rate plot of tumour-bearing mice; (e) H&E staining of the tumour and major organs in tumour-bearing mice injected with each group.

enriched into the tumor areas, when compared to that of CSP/TPE@siRNA (non-HCC-targeting NPs). The *in vivo* antitumor studies showed that CSP/TPE@siRNA-SP94 remarkably inhibited the tumor growth. Therefore, the multifunctional nanoplatform CSP/TPE@siRNA-SP94 might serve as a promising theranostic nanoplatform for HCC therapy.

Credit author statement

Hanchen Zhang: Investigation, Data curation, Resources, Writing – original draft. **Li Deng:** Investigation, Data curation, Methodology, Writing – original draft. **Haiqing Liu:** Investigation, Data curation, Validation, Resources, Visualization, Formal analysis. **Siyao Mai:** Investigation, Visualization, Data curation. **Ziliang Cheng:** Investigation, Data curation. **Guangzi Shi:** Methodology, Data curation. **Hong Zeng:** Investigation, Funding acquisition, Data curation. **Zhuo Wu:** Conceptualization, Supervision, Funding acquisition, Methodology, Project administration, Writing – review and editing.

Declaration of competing interest

The authors declare that they have no known conflict of interest that may obscure or affect their judgment to influence the work reported in this paper.

Acknowledgements

This research was supported by the National Natural Science Foundation of China (NO. 81671653), the Natural Science Foundation of Guangdong Province (NO. 2016A030313840).

Appendix A. Supplementary data

Supplementary data to this article can be found online at <https://doi.org/10.1016/j.mtbio.2022.100220>.

References

- [1] K.L. Ko, L.Y. Mak, K.S. Cheung, M.F. Yuen, Hepatocellular Carcinoma: Recent Advances and Emerging Medical Therapies, 2020, p. F1000Res 9.
- [2] A. Forner, M. Reig, J. Bruix, Hepatocellular carcinoma, *Lancet* 391 (10127) (2018) 1301–1314.
- [3] S. Li, P.E. Saw, C. Lin, Y. Nie, X. Xu, Redox-responsive polyprodrug nanoparticles for targeted siRNA delivery and synergistic liver cancer therapy, *Biomaterials* 234 (2020) 119760.
- [4] J. Ma, J. Zhang, L. Chi, C. Liu, Y. Li, H. Tian, Preparation of poly(glutamic acid) shielding micelles self-assembled from polylysine-b-polyphenylalanine for gene and drug codelivery, *Chin. Chem. Lett.* 6 (2020).
- [5] C.E. Dunbar, K.A. High, J.K. Joung, D.B. Kohn, K. Ozawa, M. Sadelain, Gene therapy comes of age, *Science* 359 (6372) (2018).
- [6] U.K. Sukumar, J.C.B. Rajendran, S.S. Gambhir, T.F. Massoud, R. Paulmurugan, SP94-Targeted triblock copolymer nanoparticle delivers thymidine kinase-p53-nitroreductase triple therapeutic gene and restores anticancer function against hepatocellular carcinoma *in vivo*, *ACS Appl. Mater. Interfaces* 12 (10) (2020) 11307–11319.
- [7] C. Su, Survivin in survival of hepatocellular carcinoma, *Cancer Lett.* 379 (2) (2016) 184–190.
- [8] Y.Y. Or, A.K. Chow, L. Ng, S.T. Fan, T.C. Yau, R.T. Poon, R.W. Pang, Survivin depletion inhibits tumor growth and enhances chemosensitivity in hepatocellular carcinoma, *Mol. Med. Rep.* 10 (4) (2014) 2025–2030.
- [9] C. Wu, F. Gong, P. Pang, M. Shen, K. Zhu, D. Cheng, Z. Liu, H. Shan, An RGD-modified MRI-visible polymeric vector for targeted siRNA delivery to hepatocellular carcinoma in nude mice, *PLoS One* 8 (6) (2013) e66416.
- [10] D. Peer, J. Lieberman, Special delivery: targeted therapy with small RNAs, *Gene Ther.* 18 (12) (2011) 1127–1133.
- [11] A. de Fougères, H.P. Vornlocher, J. Maraganore, J. Lieberman, Interfering with disease: a progress report on siRNA-based therapeutics, *Nat. Rev. Drug Discov.* 6 (6) (2007) 443–453.
- [12] Y. Lyu, M. Yu, Q. Liu, Q. Zhang, Z. Liu, Y. Tian, D. Li, M. Changdao, Synthesis of silver nanoparticles using oxidized amylose and combination with curcumin for enhanced antibacterial activity, *Carbohydr. Polym.* 230 (2020) 115573.
- [13] L.F. Siew, S.M. Man, J.M. Newton, A.W. Basit, Amylose formulations for drug delivery to the colon: a comparison of two fermentation models to assess colonic targeting performance *in vitro*, *Int. J. Pharm.* 273 (1–2) (2004) 129–134.
- [14] T. Nishimura, K. Umezaki, S.A. Mukai, S. Sawada, K. Akiyoshi, Amylose-based cationic star polymers for siRNA delivery, *BioMed Res. Int.* 2015 (2015) 962941.
- [15] T. Nishimura, K. Akiyoshi, Amylose engineering: phosphorylase-catalyzed polymerization of functional saccharide primers for glyco-biomaterials, *Wiley Interdiscip. Rev. Nanomed. Nanobiotechnol.* 9 (2) (2017).
- [16] Z. Wu, X.L. Xu, J.Z. Zhang, X.H. Mao, M.W. Xie, Z.L. Cheng, L.J. Lu, X.H. Duan, L.M. Zhang, J. Shen, Magnetic cationic amylose nanoparticles used to deliver survivin-small interfering RNA for gene therapy of hepatocellular carcinoma *in vitro*, *Nanomaterials* 7 (5) (2017).
- [17] H. Kobayashi, R. Watanabe, P. Choyke, Improving conventional enhanced permeability and retention (EPR) effects; what is the appropriate target? *Theranostics* 4 (1) (2013) 81–89.
- [18] E. Ruoslahti, Tumor penetrating peptides for improved drug delivery, *Adv. Drug Deliv. Rev.* (2017) 3–12.
- [19] M. Liang, C. Gao, Y. Wang, W. Gong, S. Fu, L. Cui, Z. Zhou, X. Chu, Y. Zhang, Q. Liu, X. Zhao, B. Zhao, M. Yang, Z. Li, C. Yang, X. Xie, Y. Yang, C. Gao, Enhanced blood-brain barrier penetration and glioma therapy mediated by T7 peptide-modified low-density lipoprotein particles, *Drug Deliv.* 25 (1) (2018) 1652–1663.
- [20] M. Yu, W. Pang, T. Yang, J. Wang, L. Wei, C. Qiu, Y. Wu, W. Liu, W. Wei, X. Guo, Q. Zhang, Systemic delivery of siRNA by T7 peptide modified core-shell nanoparticles for targeted therapy of breast cancer, *Eur. J. Pharmaceut. Sci.* 92 (2016) 39–48.
- [21] M. Riaz, X. Zhang, K. Wong, H. Chen, Q. Liu, X. Chen, G. Zhang, A. Lu, Z. Yang, Pulmonary delivery of transferrin receptors targeting peptide surface-functionalized liposomes augments the chemotherapeutic effect of quercetin in lung cancer therapy, *Int. J. Nanomed.* 14 (2019) 2879–2902.
- [22] Y. Lu, W. Jiang, X. Wu, S. Huang, Z. Huang, Y. Shi, Q. Dai, J. Chen, F. Ren, S. Gao, Peptide T7-modified polypeptide with disulfide bonds for targeted delivery of plasmid DNA for gene therapy of prostate cancer, *Int. J. Nanomed.* 13 (2018) 6913–6927.
- [23] R. Wang, Y. Hu, Y. Yang, W. Xu, M. Yao, D. Gao, Y. Zhao, S. Zhan, X. Shi, X. Wang, Using PEGylated iron oxide nanoparticles with ultrahigh relaxivity for MR imaging of an orthotopic model of human hepatocellular carcinoma, *J. Nanoparticle Res.* 19 (2) (2017) 12.
- [24] A. Lo, C.T. Lin, H.C. Wu, Hepatocellular carcinoma cell-specific peptide ligand for targeted drug delivery, *Mol. Cancer Therapeut.* 7 (3) (2008) 579–589.
- [25] B. Jiang, R. Zhang, J. Zhang, Y. Hou, X. Chen, M. Zhou, X. Tian, C. Hao, K. Fan, X. Yan, GRP78-targeted ferritin nanocaged ultra-high dose of doxorubicin for hepatocellular carcinoma therapy, *Theranostics* 9 (8) (2019) 2167–2182.
- [26] A.S. Lee, The glucose-regulated proteins: stress induction and clinical applications, *Trends Biochem. Sci.* 26 (8) (2001) 504–510.
- [27] Y. Qu, J. Li, J. Ren, J. Leng, C. Lin, D. Shi, Enhanced magnetic fluid hyperthermia by micellar magnetic nanoclusters composed of Mn(x)Zn(1-x)Fe(2)O(4) nanoparticles for induced tumor cell apoptosis, *ACS Appl. Mater. Interfaces* 6 (19) (2014) 16867–16879.
- [28] H. Yang, Y. He, Y. Wang, R. Yang, N. Wang, L.M. Zhang, M. Gao, X. Jiang, Theranostic nanoparticles with aggregation-induced emission and MRI contrast enhancement characteristics as a dual-modal imaging platform for image-guided tumor photodynamic therapy, *Int. J. Nanomed.* 15 (2020) 3023–3038.
- [29] L.R. Roberts, C.B. Sirlin, F. Zaiem, J. Almasri, L.J. Prokop, J.K. Heimbach, M.H. Murad, K. Mohammed, Imaging for the diagnosis of hepatocellular carcinoma: a systematic review and meta-analysis, *Hepatology* 67 (1) (2018) 401–421.
- [30] Y.D. Xiao, R. Paudel, J. Liu, C. Ma, Z.S. Zhang, S.K. Zhou, MRI contrast agents: classification and application (Review), *Int. J. Mol. Med.* 38 (5) (2016) 1319–1326.
- [31] W. Xie, Z. Guo, F. Gao, Q. Gao, D. Wang, B.S. Liaw, Q. Cai, X. Sun, X. Wang, L. Zhao, Shape-, size- and structure-controlled synthesis and biocompatibility of iron oxide nanoparticles for magnetic theranostics, *Theranostics* 8 (12) (2018) 3284–3307.
- [32] Z. Gao, T. Ma, E. Zhao, D. Docter, W. Yang, R.H. Stauber, M. Gao, Small is smarter: nano MRI contrast agents - advantages and recent achievements, *Small* 12 (5) (2016) 556–576.
- [33] J. Lu, J. Wang, D. Ling, Surface engineering of nanoparticles for targeted delivery to hepatocellular carcinoma, *Small* 14 (5) (2018).
- [34] J.H. Wang, A.N. Endsley, C.E. Green, A.C. Matin, Utilizing native fluorescence imaging, modeling and simulation to examine pharmacokinetics and therapeutic regimen of a novel anticancer prodrug, *BMC Cancer* 16 (2016) 524.
- [35] Z.J. Li, C. Li, M.G. Zheng, J.D. Pan, L.M. Zhang, Y.F. Deng, Functionalized nanographene oxide particles for targeted fluorescence imaging and phototherapy of glioma U251 cells, *Int. J. Clin. Exp. Med.* 8 (2) (2015) 1844–1852.
- [36] L. Yan, Y. Zhang, B. Xu, W. Tian, Fluorescent nanoparticles based on AIE fluorogens for bioimaging, *Nanoscale* 8 (5) (2016) 2471–2487.
- [37] Z. Zhao, D. Liu, F. Mahtab, L. Xin, Z. Shen, Y. Yu, C.Y. Chan, P. Lu, J.W. Lam, H.H. Sung, I.D. Williams, B. Yang, Y. Ma, B.Z. Tang, Synthesis, structure, aggregation-induced emission, self-assembly, and electron mobility of 2,5-bis(triphenylsilyl)ethyl-3,4-diphenylsiloles, *Chemistry* 17 (21) (2011) 5998–6008.
- [38] Z. Wang, S. Chen, J.W. Lam, W. Qin, R.T. Kwok, N. Xie, Q. Hu, B.Z. Tang, Long-term fluorescent cellular tracing by the aggregates of AIE bioconjugates, *J. Am. Chem. Soc.* 135 (22) (2013) 8238–8245.
- [39] Y. Ma, S. Tong, G. Bao, C. Gao, Z. Dai, Indocyanine green loaded SPIO nanoparticles with phospholipid-PEG coating for dual-modal imaging and photothermal therapy, *Biomaterials* 34 (31) (2013) 7706–7714.
- [40] Q. Hu, X. Gao, T. Kang, X. Feng, D. Jiang, Y. Tu, Q. Song, L. Yao, X. Jiang, H. Chen, J. Chen, CGKRK-modified nanoparticles for dual-targeting drug delivery to tumor cells and angiogenic blood vessels, *Biomaterials* 34 (37) (2013) 9496–9508.
- [41] B. Tombach, P. Reimer, C. Bremer, T. Altkemper, M. Engelhardt, M. Mahler, W. Ebert, W. Heindel, First-pass and equilibrium-MRA of the aortiliac region with a superparamagnetic iron oxide blood pool MR contrast agent (SH U 555 C): results of a human pilot study, *NMR Biomed.* 17 (7) (2004) 500–506.

- [42] M. Taupitz, S. Wagner, J. Schnorr, I. Kravec, H. Pilgrimm, H. Bergmann-Fritsch, B. Hamm, Phase I clinical evaluation of citrate-coated monocrystalline very small superparamagnetic iron oxide particles as a new contrast medium for magnetic resonance imaging, *Invest. Radiol.* 39 (7) (2004) 394–405.
- [43] S.D. Conner, S.L. Schmid, Regulated portals of entry into the cell, *Nature* 422 (6927) (2003) 37–44.
- [44] Q. Wang, H. Yan, Y. Jin, Z. Wang, W. Huang, J. Qiu, F. Kang, K. Wang, X. Zhao, J. Tian, A novel plectin/integrin-targeted bispecific molecular probe for magnetic resonance/near-infrared imaging of pancreatic cancer, *Biomaterials* 183 (2018) 173–184.